AN INTEGRATED LOADS ANALYSIS MODEL FOR WAKE VORTEX ENCOUNTERS

Thiemo M. Kier[1]

[1]German Aerospace Center
DLR-Oberpfaffenhofen
Institute of System Dynamics and Control
82234 Wessling, GERMANY
Thiemo.Kier@dlr.de

Keywords: Gust Loads Analysis, Unsteady aerodynamics, Rational function approximation, Nonlinear time domain simulation, Wake vortex encounter.

Abstract: When a plane crosses the wake generated by a preceding aircraft, large dynamical loads in the order of the design loads may be induced. Loads analysis models for such wake vortex encounters need to consider aspects important for manoeuvre, as well as gust type responses. If the angle between the path and the trailing vortices is small, the encounter is manoeuvre like due to large induced roll motion. When the vortices are crossed almost perpendicularly, a gust type response is to be expected, where unsteady aerodynamic effects are significant. In [1] a modeling approach of an integrated loads analysis model suitable for wake vortex encounters was presented. This contribution will further investigate the requirements for such flight loads models for wake vortex encounters. One important aspect is, that the bandwidth of the excitation due to gust type wake vortex encounters is considerably larger compared to classical design gusts. Hence, the convergence behavior for high reduced frequencies of the doublet lattice models needs to be examined in more detail. A rational function approximation (RFA) is required to make the unsteady aerodynamics amendable for nonlinear time domain simulations. Previously, a "physical" RFA could significantly improve the results for incompressible flow at high reduced frequencies by explicit approximation of the added mass term. The "physical" RFA scheme is now extended to the compressible regime. The results are compared to the solution of the Possio equation and a velocity potential method for unsteady motion of airfoils in compressible flow.

Further, the (time domain) integral loads analysis model is compared to a frequency domain approach. Induced velocities due to a pre-described trajectory for a wake crossing are determined. A subsequent Fourier transformation yields the excitation spectrum for the frequency domain calculations. Various encounter angles with wake vortices are computed and compared to time domain simulations, where the trajectory is determined as a nonlinear response during the simulation. Results show that in some encounter scenarios these nonlinearities can become crucial.

1 INTRODUCTION

Flight loads analysis models need to satisfy different requirements depending if a dynamic response due to a manoeuvre or a gust is considered. The manoeuvre model needs to capture large angles and displacements of the rigid body and nonlinearities in the aerodynamic data, similarly to flight mechanical simulations. Hence, these models are usually simulated in the time domain using integration of the underlying ordinary differential equations. Gust response models need to include unsteady aerodynamics due to

the rapid change of the inflow conditions. The resulting rigid body response is usually small compared to manoeuvre. Further, the data for unsteady aerodynamics is typically computed as a function of reduced frequency. Hence, the loads analysis for the gust case can be considered as a linear problem, which can be conveniently solved in the frequency domain.

Occasionally, events beyond the scope of the design load cases specified in the regulations CS 25 [2] are of interest. In some instances, it is indispensable, to consider a combination of gusts and manoeuvres. The developement of an integral loads analysis model capable of handling such cases, has been described in a series of papers [3–5]. The basis of these models is a suitable set of equations of motion for structural dynamics with large rigid body motion, and a rational function approximation (RFA) of the frequency dependent aerodynamic influence coefficient (AIC) matrices. This allows for a transformation of the unsteady aerodynamics to the Laplace domain and thus is amendable to time domain integration.

Wake vortex encounters (WVE) are a prime example, where, depending on the encounter scenario, either large roll angles of the encountering aircraft can be induced, or significant unsteady aerodynamics effects need to be considered. In [1] the two limiting cases of WVE scenarios were simulated. An encountering angle of $\Psi = 0$ deg resulting in large rolling movement and a perpendicular crossing with an angle of $\Psi = 90$ deg with significant unsteadiness of the flow.

The flow field of a WVE is three dimensional, i.e. the gust velocities depend on all three spatial coordinates, compared to the only one dimensional velocity field as specified for the discrete gust in paragraph CS 25.341 of the regulations. Further, the gust velocity field of a WVE has very large spatial gradients.

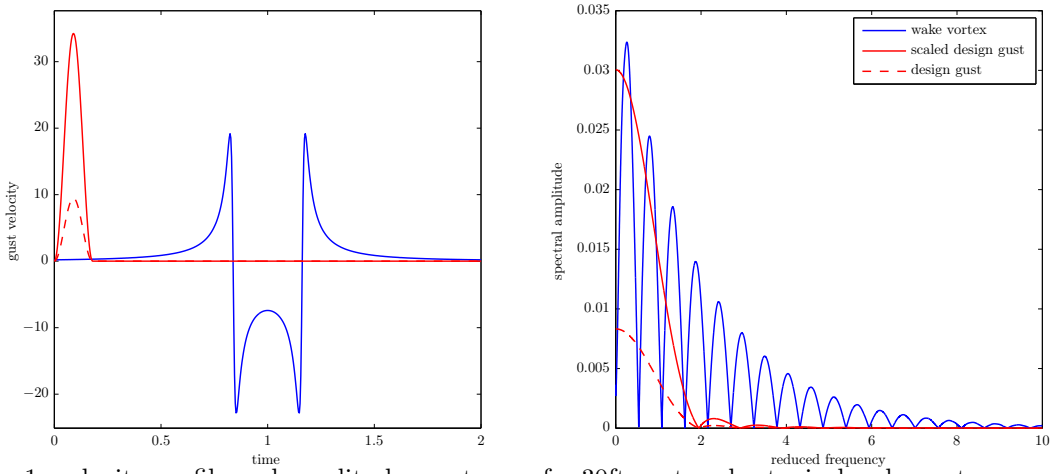

Figure 1: velocity profile and amplitude spectrum of a 30ft gust and a typical wake vortex encounter

The consequences are twofold. Firstly, the frequency content of a WVE is significantly higher compared to even the shortest 1-cos design gust. The left of Figure 1 compares the 1D velocity profile of a 30 ft design gust with a typical WVE. The right subfigure depicts their amplitude spectrum, where the 30 ft gust is scaled to yield the same power spectral density. Clearly, much higher reduced frequencies need to be considered in the WVE case. Of course, these values are highly scenario dependent and are depicted for illustration only.

Secondly, the induced velocities depend nonlinearly on the flight path. The gust velocities of a pre-computed path might be invalid and an online position and attitude dependent calculation becomes necessary. These two issues will be addressed in this paper.

A short review of the involved model equations is presented. This is followed by a comparison of high reduced frequency aerodynamic methods for thin 2D airfoils, in order to validate the doublet lattice method (DLM) and the corresponding RFA for the frequency range in question.

Thereafter, wake vortex crossings with encounter angles ranging from 90 to 10 degrees are investigated. A transport aircraft with a T-tail was chosen as example, because of its interesting dynamic response characteristics.

Very often, it is questioned whether the method of rational function approximations is able to correctly reproduce the frequency domain aerodynamics. To assess the adequacy of the RFA, fixed path wake vortex encounters were computed in the frequency domain. The excitation spectrum is set up using a Fourier transformed time signal of the wake induced velocities using the same routine as used in the nonlinear simulations. AIC matrices evaluated from the RFA are compared to ones that are directly computed by the DLM. Inverse Fourier transformation then yields the time responses of the load output stations.

Finally, the importance of the nonlinear position dependence of the aircraft wrt the wind field is examined. A time domain simulation was performed. The resulting nonlinear trajectory was used to calculate a spectrum of the downwash and compared to a pre-calculated straight trajectory. Again, the responses are compared in the time domain using inverse Fourier transformation. This allows the validation of the time domain simulation versus the frequency domain calculation and the influence on the loads of fixed versus time dependent trajectories.

2 MODEL EQUATIONS FOR LOADS ANALYSIS

2.1 Equations of Motion

The starting point, when setting up the equations of motion (EOM) for a loads analysis model for a flexible aircraft is a dynamic finite element model (FEM). To reduce the problem size, the dynamic FEM is reduced using Guyan's method [6], where condensation points ($g-set$) are placed along a loads reference axis. Subsequently, a modal analysis is carried out and only part of the modal basis covering the frequency range of interest is retained, to further reduce the computational cost.

The eigenvalues and eigenvectors define the generalized coordinates of the $h-set$. The zero eigenvalues represent the rigid body motion. The $h-set$ can be partitioned into rigid body DOFs ($b-set$) and flexible part ($f-set$). The mode shapes $\mathbf{\Phi}_{gb}$, respectively $\mathbf{\Phi}_{gf}$ are then used to generalized the equations of motion, which are given in the frequency domain by

$$\left\{-\omega^2 \begin{bmatrix} \mathbf{M}_{bb} & \mathbf{0} \\ \mathbf{0} & \mathbf{M}_{ff} \end{bmatrix} + \mathrm{i}\,\omega \begin{bmatrix} \mathbf{0} & \mathbf{0} \\ \mathbf{0} & \mathbf{B}_{ff} \end{bmatrix} + \begin{bmatrix} \mathbf{0} & \mathbf{0} \\ \mathbf{0} & \mathbf{K}_{ff} \end{bmatrix}\right\} \begin{bmatrix} \mathbf{u}_b \\ \mathbf{u}_f \end{bmatrix} = \begin{bmatrix} \mathbf{\Phi}_{gb}^{\mathrm{T}} \\ \mathbf{\Phi}_{gf}^{\mathrm{T}} \end{bmatrix} \mathbf{P}_g^{ext}(\omega). \qquad (1)$$

A suitable set of equations of motion to account for large rigid body motions and linear flexibility is derived in the references [7–10], which describe the movement relative to a "mean axes" body reference frame. Then, the EOM are given as

$$\begin{aligned} \begin{bmatrix} \mathbf{m}_b \left(\dot{\mathbf{V}}_b + \boldsymbol{\Omega}_b \times \mathbf{V}_b - \mathbf{T}_{bE}\, \mathbf{g}_E \right) \\ \mathbf{J}_b \dot{\boldsymbol{\Omega}}_b + \boldsymbol{\Omega}_b \times (\mathbf{J}_b \boldsymbol{\Omega}_b) \end{bmatrix} &= \boldsymbol{\Phi}_{gb}^{\mathrm{T}} \mathbf{P}_g^{ext}(t) \\ \mathbf{M}_{ff} \ddot{\mathbf{u}}_f + \mathbf{B}_{ff} \dot{\mathbf{u}}_f + \mathbf{K}_{ff} \mathbf{u}_f &= \boldsymbol{\Phi}_{gf}^{\mathrm{T}} \mathbf{P}_g^{ext}(t), \end{aligned} \tag{2}$$

where $\mathbf{V}_b$ and $\boldsymbol{\Omega}_b$ are the velocity, respectively angular velocity in the body frame of reference. The matrix $\mathbf{T}_{bE}$ transforms the gravitational vector from an earth fixed (E) to a body fixed coordinate frame (b).

2.2 Aerodynamic Influence Coefficient Matrices

The major contribution to the excitation forces $\mathbf{P}_g^{ext}$, stem from the aerodynamics. Classical aerodynamic methods based on potential theory provide Aerodynamic Influence Coefficient (AIC) matrices, which allow a closed form expression with the equations of motion (1) and (2).

The Vortex Lattice Method (VLM) [11] discretizes a lifting surface by trapeziodal shaped elementary wings, so called aerodynamic boxes. The aerodynamic lift is generated by placing a so called horseshoe vortex along the quarter chord line of such an aerodynamic box. The circulation strength $\boldsymbol{\Gamma}_j$ of the individual vortices is determined using the Biot-Savart-Law by meeting the flow tangency condition at the 3/4 chord of each box. The

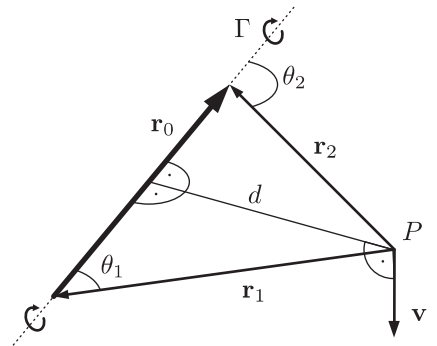

Figure 2: Biot-Savart-Law for a straight vortex filament

induced velocity for a straight vortex filament with the geometrical properties illustrated in figure 2, is given by

$$\mathbf{v} = \frac{\Gamma}{4\pi} \frac{\mathbf{r}_1 \times \mathbf{r}_2}{|\mathbf{r}_1 \times \mathbf{r}_2|^2 + r_c^2 |\mathbf{r}_0|^2} \left(\mathbf{r}_0 \cdot \left(\frac{\mathbf{r}_1}{|\mathbf{r}_1|} - \frac{\mathbf{r}_2}{|\mathbf{r}_2|} \right) \right), \tag{3}$$

where r_c is the radius of a viscous core.

Calculating the influence of each horseshoe vortex on every collocation point results in a matrix, which can be inverted to determine the circulation strengths when satisfying the flow tangency condition. This allows to formulate a direct relationship between the normalwash at the control point and the box-pressure.

$$\Delta \mathbf{c}_{\mathbf{p}_j} = \mathbf{Q}_{jj}\, \mathbf{w}_j \tag{4}$$

The matrix $\mathbf{Q}_{jj}$ is the so called AIC matrix.

To account for a rapidly changing normalwash, unsteady aerodynamics need to be considered. Therefore, the Doublet Lattice Method [12, 13] (DLM) is employed, which is an unsteady extension to the steady VLM. The governing flow equation is the unsteady Prandtl-Glauert equation (5), which differs from its steady counter part by the presence of the partial derivatives wrt to time.

$$\left(1 - Ma_\infty^2\right) \frac{\partial^2 \Phi}{\partial x^2} + \frac{\partial^2 \Phi}{\partial y^2} + \frac{\partial^2 \Phi}{\partial z^2} - \left(2 \frac{Ma_\infty}{a_\infty}\right) \frac{\partial^2 \Phi}{\partial x \partial t} - \left(\frac{1}{a_\infty^2}\right) \frac{\partial^2 \Phi}{\partial t^2} = 0 \tag{5}$$

The Doublet Lattice Method (DLM) provides a harmonic solution for this equation. Further, is uses the acceleration potential which is formally equivalent to the velocity potential equation. Therefore, the same elementary solutions are valid, e.g. the doublet potential. The acceleration potential readily yields the pressure difference between the upper and lower surface. Since there is no pressure jump across the wake, it can be omitted in the modeling process. The final result for the unsteady AIC matrix $\mathbf{Q}_{jj}(k)$ has the same form as its steady counterpart, however additionally it depends on the reduced frequency $k = \frac{c_{ref}/2}{U_\infty}\omega$.

To calculate the pressure difference, the motion or gust induced normal wash at the three-quarter-chord point ($j - set$) needs to be determined. The reference point of an aerodynamic box is its mid point and denoted by the $k - set$. The matrix $\mathbf{S}_{kj}$ converts the pressures to discrete loads at the mid chord location. The flow conditions can be expressed as a function of reduced frequency, in terms of the displacements of the $k - set$.

$$\mathbf{w}_j(k) = \left(\mathbf{D^x}_{jk} + \mathrm{i}k\, \mathbf{D^t}_{jk}\right)\, \mathbf{u}_k(k), \tag{6}$$

where $\mathbf{D^x}_{jk}$ is a differentiation in x-direction, i.e., yields the normalwash contribution due to a change in local angle of attack and $\mathrm{i}k\ \mathbf{D^t}_{jk}$ is a differentiation wrt time, i.e. the contribution due to a heaving motion.

The interconnection of the aerodynamic grid ($k - set$) to the structural grid ($g - set$) is given by the so called spline matrix $\mathbf{T}_{kg}$. The interpolation scheme employed to create this spline matrix, is commonly based on radial basis functions such as e.g. the Infinite Plate Spline (IPS) [14].

2.3 Rational Function Approximation

The doublet lattice method provides aerodynamic matrices as tabulated values at discrete reduced frequencies. One possibility to make them amendable for time domain integration, is the so called rational function approximation (RFA), where the frequency domain transfer functions are fit with suitable "rational" terms. These can then be Laplace transformed and cast in state space form. Many flavors of this method have been published in literature [15–18]. Most of these publications concentrate on approximation of the generalized aerodynamic matrices $\mathbf{Q}_{hh}$, i.e. the AIC matrices are already post-multiplied with the differentiation matrices (6) and the modal basis. While this approach reduces the computational cost considerably due to a smaller problem size, fitting of the AICs $\mathbf{Q}_{jj}(k)$ without multiplication with differentiation matrices has been proposed in [5]:

$$\mathbf{Q}_{jj}(s^*) = \mathbf{Q^0}_{jj} + \mathbf{Q^1}_{jj} s^* + \sum_{i=1}^{n_p} \mathbf{Q^{L_i}}_{jj} \frac{s^* \mathbf{I}}{s^* + p_i}, \tag{7}$$

where $s^* = s\left(\frac{c_{ref}/2}{U_\infty}\right)$ is the Laplace domain equivalent to the reduced frequency k. The reason for the presence of a second derivative in the classical RFA compared to the present formulation, is the additional time derivative in the downwash equation (6). The present, "physical" RFA (7) has several advantages over the approximation of the generalized aerodynamic forces. E.g., the fit is not tied to a particular mass case. But more importantly, the individual terms of the fit allow a physical interpretation. The term $\mathbf{Q^0}_{jj}$ represents the quasi-steady term, $\mathbf{Q^1}_{jj}$ is the added mass (in incompressible flow), and the terms $\mathbf{Q^{L_i}}_{jj}$ with the predefined poles p_i, are responsible for the lagging behavior of the unsteady flow. In [1] a method for numerically calculation of the incompressible added mass term was proposed. Further, this fit also allows the consideration of a nonlinear position dependence of the wind field as demonstrated in [1], since the normalwash $\mathbf{w}_j$ can be computed online and fed into a realization of the ordinary differential equations (ODE) (8) of the unsteady aerodynamics in order to determine the so called lag states $\mathbf{x}_L$.

$$\dot{\mathbf{x}}_L = \tfrac{U_\infty}{c_{ref}/2}\mathbf{R}\,\mathbf{x}_L + \mathbf{E}\,\dot{\mathbf{w}}_j \tag{8}$$

The matrices $\mathbf{R}$ and $\mathbf{E}$ are stacked diagonal matrices, containing the poles p_i, respectively identity matrices. The splined aerodynamic forces including steady the unsteady parts are then

$$\mathbf{P}_g^{aero} = \underbrace{\left(\mathbf{Q^0}_{gj}\,\mathbf{w}_j\right)}_{\text{steady } \mathbf{P}_g^s(\mathbf{w}_j)} + \underbrace{\left(\mathbf{Q^1}_{gj}\left(\tfrac{c_{ref}/2}{U_\infty}\right)\,\dot{\mathbf{w}}_j + \mathbf{D}\,\mathbf{x}_L(\dot{\mathbf{w}}_j)\right)}_{\text{unsteady } \mathbf{P}_g^u(\dot{\mathbf{w}}_j)}, \tag{9}$$

where $\mathbf{D}$ contains the coefficients $\mathbf{Q^{L_i}}_{gj}$ from the least squares procedure according to Roger. With the "physical" RFA it is possible to discern between the steady and unsteady contribution of the aerodynamics.

3 HIGH REDUCED FREQUENCY COMPRESSIBLE AIRFOIL AERODYNAMICS

When high reduced frequency unsteady aerodynamics are required, as in the case of wake vortex encounters, the question arises whether the applied methods are able to predict the unsteady pressure distribution with an acceptable accuracy. The two methods in question used in the current modeling scheme, are firstly the DLM to generate the aerodynamic matrices and secondly the RFA to approximate them in the Laplace domain.

In [19] analytical expressions for the pressure distributions of 2D airfoils in unsteady motion and incompressible flow where derived. In [1] these expressions were compared to pressures from a DLM and an RFA of the DLM pressures. Remarkably, the extrapolation of the RFA to very high frequencies gave a better result than a direct DLM calculation. The structure of the "physical" RFA was able to fit the added mass term, which is the dominating term in the high frequency range, where the lower frequencies of the DLM were still reliable. A direct DLM calculation however would require a very fine discretization to capture high frequencies.

Now this comparison needs to be extended to compressible flow, i.e. for Mach numbers greater zero. The physics of compressible flow changes in that respect, that now the pressures travel in waves with a finite speed of sound a_∞, whereas in the incompressible case, the lagging behavior was purely confined to the convection of the wake. For compressible flow these traveling waves add another source of time dependence. A direct consequence

of this is that the added mass term is no longer directly proportional to the acceleration in the fluid, but also has a transfer behavior. The unsteady Prandtl-Glauert equation (5) can be subjected to the following transformation:

$$\Phi(x, y, z, t) = \varphi(X, Y, Z) \cdot \exp\left(\mathrm{i}k\frac{Ma^2}{1 - Ma^2}X + k\tau\right), \tag{10}$$

which yields as result the Helmholtz equation

$$\nabla^2\varphi + \kappa^2\varphi = 0, \quad \text{with} \quad \kappa = k\frac{Ma}{1 - Ma^2}, \tag{11}$$

which is indicative of the wave like behavior. For steady ($k = 0$) or incompressible ($Ma = 0$) flow, the problem reduces to the Laplacian equation $\nabla^2\varphi = 0$.

Unfortunately, analytical solutions for compressible unsteady pressure distributions of airfoils do not exist, therefore, numerical procedures have to be considered. In [20] a method for solving Possio's equation is presented. A computational routine was setup to yield aerodynamic influence coefficients, with which pressure distributions for arbitrary excitations can be computed. Further, a compressible 2D Velocity Potential Method (VPM) has been implemented, using fundamental solutions of the two dimensional incarnation of the Helmholtz equation (11) based on Greens functions $G_\kappa = \frac{\mathrm{i}}{4}H_0^{(1)}(\kappa r)$ for $\kappa > 0$ and $G_0 = -\frac{1}{2\pi}\log r$ for $\kappa = 0$. The velocity potential requires the modelling of the wake, therefore, the airfoil and the wake are discretized by linear doublet panels. Differentiating the Greens functions twice, yields the induced velocity due to a point doublet, which is integrated over the panel length by a Gaussian quadrature. Special attention is required for the self-influence of the doublet panels, because of the hyper-singular nature of the kernel. For $\kappa = 0$ the doublet panel reduces to double vortices at the panel edges. When only the airfoil is discretized, this yields the added mass term as derived in [1]. With the same numerical scheme a compressible non-circulatory term can be calculated for $\kappa > 0$, which corresponds to the added mass for the incompressible case. However, now this term is frequency dependent.

For the RFA equation (7), this means that the term $\mathbf{Q^1}_{jj}$ vanishes and, will have to be approximated with lag terms instead. The number of poles will have to be increased, since two different propagation mechanisms at different time scales are at work, the convection of the wake and the propagation of the waves due to the finite speed of sound. From which Mach number on, it is useful to drop the added mass term in favor of additional lag terms, and whether it is beneficial to separately approximate the non-circulatory terms, is still subject of investigation.

For the numerical comparison an evenly spaced DLM symmetric half model of a straight wing ($AR = 20$) with 24 panels in chordwise and 96 panels in spanwise direction was set up. The inner most strip is used for the comparison to the 2D methods. The Possio solver uses 51 collocation points in a cosine spacing. The 2D velocity potential method uses 100 panels on the airfoil and a wake-length of 10 chords. Further, an RFA with 15 poles was applied to $\mathbf{Q}_{jj}(k)$ from the Possio solver, which is believed to be the most accurate result. Figure 3 shows imaginary and real parts of the pressure distributions for heave, pitch and flap motion. Additionally, the pressure distributions for sinusoidal gusts were computed. The chosen Mach number is $Ma = 0.6$ and the displayed reduced frequency is $k = 3.0$.

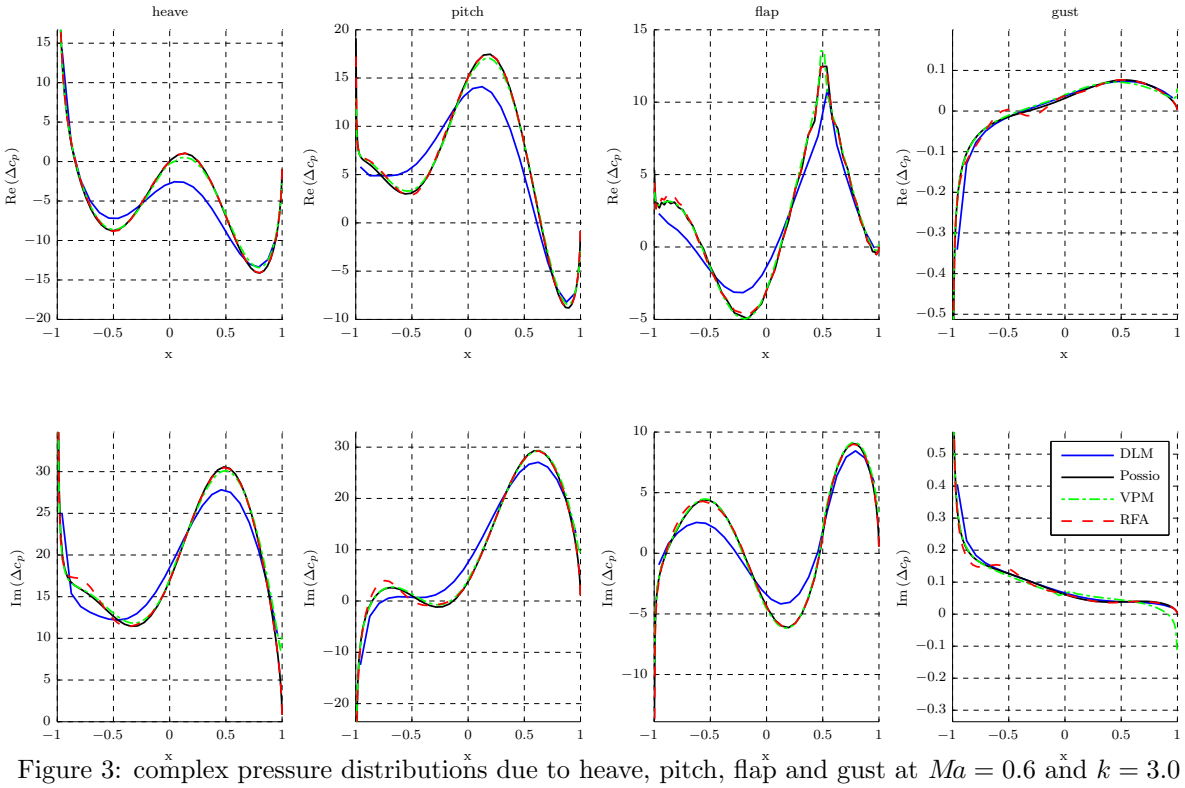

Figure 3: complex pressure distributions due to heave, pitch, flap and gust at $Ma = 0.6$ and $k = 3.0$

The pressures become quite wavy, as this is already a quite large reduced frequency. This also explains the requirement for a relatively large amount of poles for an RFA. The DLM is not quite able to follow in the cases of heave pitch and flap motion. Agreement for the gust pressures however is very good. For the WVE case this is a favorable result, since the rigid motions are associated with lower frequency excitation of the structure, whereas the requirement for high reduced frequencies stem from the gust excitation of the wind-field.

In figure 4 integral values for lift and moment are displayed in the complex plane for flap and gust excitation. The flap case demonstrates that the RFA is able to follow the spiraling nature of the values. As expected the moments are more difficult to approximate than the lift, but overall a very good agreement could be achieved. For the rigid body motions, the DLM is only accurate up to a reduced frequency of about $k = 3.0$, but since the excitation of the structure is confined to lower frequencies, this behavior is deemed acceptable. It also has to be stressed that the 3D DLM method with a rather coarse grid spacing is compared to pure 2D methods with a significantly finer discretization.

The gust case is of particular interest for the WVEs and shows a very good agreement of the DLM and RFA even at high reduced frequencies. The VPM has some problems in the lower frequency range, probably due to a mismatch of excitation and discretization.

It can be concluded that the DLM is able to provide data suitable for the high frequencies of gust excitation due to a wake vortex encounter. Further, the RFA is capable of capturing even spiral type behavior in the complex plane, at the expense of additional poles for the compressible case.

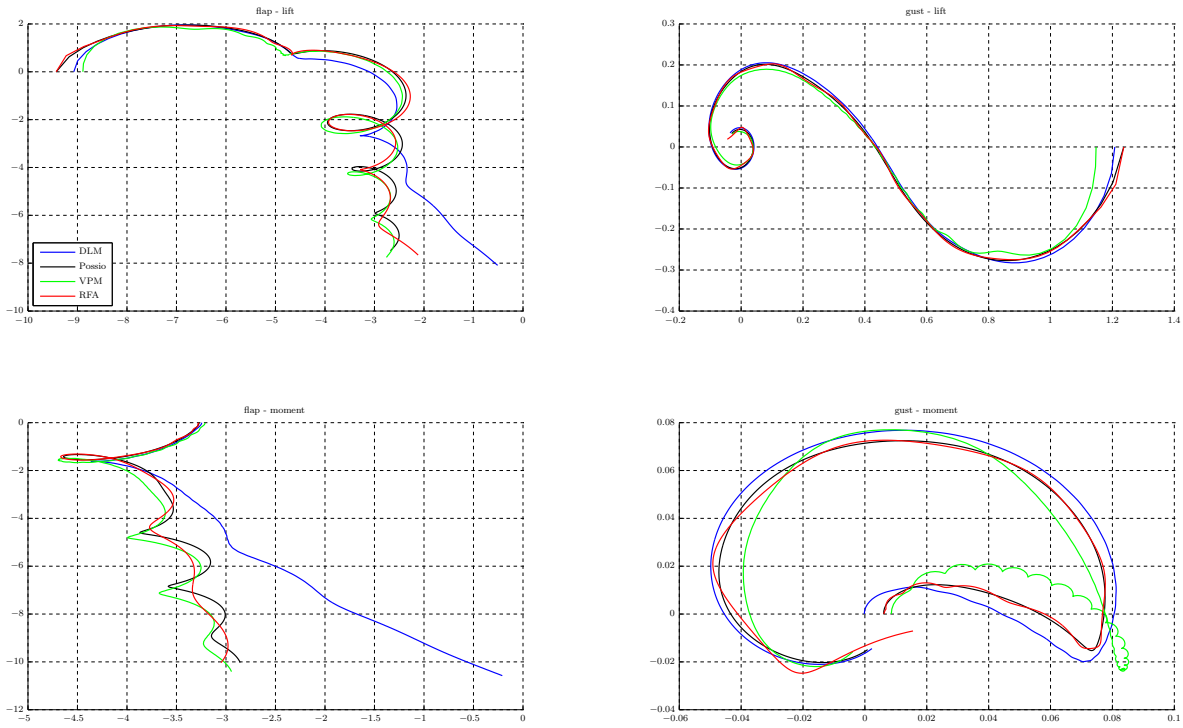

Figure 4: Lift and moment due to flap and gust in the complex plane up to $k_{max} = 10$

4 WAKE VORTEX ENCOUNTERS

As encountering aircraft, a transport aircraft with a T-Tail was chosen. The fact that the lowest frequency modes are typically the bending and torsion of the tail, rather than the wing, provides for interesting dynamic responses in wake vortex encounters. The interest in loads for these types of aircraft was also triggered by flight tests for formation flying [21] of C-17 Globemaster to reduce fuel consumption, where encounters are probable due to the proximity to the vortex of the preceding aircraft. Also, in tactical missions such wake vortex encounters are much more likely compared to commercial aviation, where great effort is undertaken to predict and avoid wakes of other aircraft [22].

4.1 Parameterization of the Encounter Scenarios

Of course a multitude of encounter scenarios are possible, with different ages of the wake and different orientation of the encountering aircraft to the wake system. Therefore, some simplifying assumptions regarding the parameter space are imposed. First the wake parameters are defined. The wake vortex strength of the generating aircraft is defined by

$$\Gamma_w = \frac{W_G n_z}{\rho V_G b_w}. \tag{12}$$

After a short time, the trailing vortices released at the wing tips shift inboards due to self induced velocities. After that, the distance b_w between the trailing vortices of the wake is assumed to remain constant. The core radius for a young but fully developed vortex is approximately $r_c \approx 0.0275 \cdot b_w$. The three values Γ_w, b_w, and r_c constitute the basic properties of the wake.

The parameters of the encounter are defined by Euler angles $(\phi, \theta, \psi)_w$ of the wake to orient it in a geodetic frame of reference, and a vertical offset h to adjust the height. The

encountering aircraft is placed at some distance in a trimmed state with a heading of $\psi_E = 0$. The values θ_w and ϕ_w can be used to mimic a roll angle during the encounter, respectively a vertical offset between the right and left vortex.

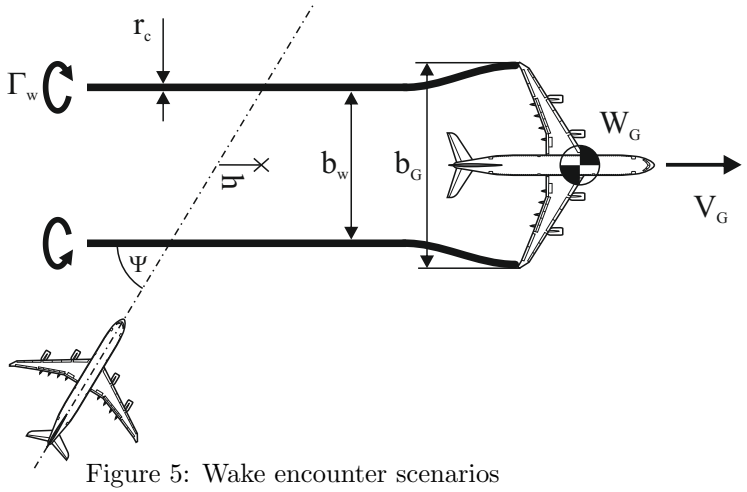

Figure 5: Wake encounter scenarios

For the present study θ_w and ϕ_w are set to zero. ψ_w then corresponds directly to an encounter angle, as depicted in figure 5. A sweep of encounter angles from 90 deg to 10 deg was simulated. The aerodynamics of the encountering aircraft was modified in such a way, that the trim angle of attack is zero. This allows an easier interpretation of the results. The Mach number was set to 0.3 at sea level.

4.2 Frequency Domain Approach for WVE

To asses the accuracy of the rational function approximation, a comparison with the tabulated unsteady aerodynamics was conducted in the frequency domain. For this comparison a frequency domain calculation of wake vortex encounters was set up. As the flow field of an WVE is three-dimensional as opposed to the one dimensional design gust, the determination of the excitation spectrum warrants further discussion.

A cut in the y-z plane of the wake induced velocity field is depicted in figure 6. Using

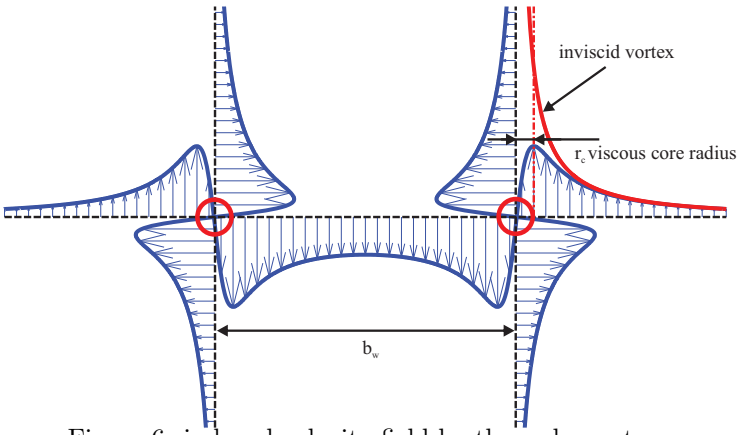

Figure 6: induced velocity field by the wake vortex

predefined trajectory data, i.e. the position $(x, y, z)_E$ and attitude $(\phi, \theta, \psi)_E$ of the encountering aircraft, the wake is transformed from the earth fixed to the aircraft body fixed

coordinate system. The Biot-Savart equation (3) is then used to determine the induced normalwash $\mathbf{w}_j(t)$ of the wake at every control point for each time step. A subsequent Fourier transformation yields the spectrum of the wake vortex encounter $\mathbf{w}_j^{WVE}(k)$. The maximum frequency and number of frequencies have to be chosen to ensure a satisfactory resolution. Multiplication with the AIC matrix $\mathbf{Q}_{gj}(k)$ for each reduced frequency and the dynamic pressure, results in a frequency response function for the excitation $\mathbf{P}_g^{WVE}(\omega)$. This excitation column is used in the linear EoM (1) and solved for the modal displacements and the loads at defined output stations. Inverse Fourier transformation allows for comparison with the time domain simulations.

4.3 Unsteady Aerodynamics for WVE

Initially, the vertical offset h is chosen such, that the cores of the vortices directly impact the horizontal stabilizer of the T-tail. A fixed path frequency domain calculation for the encounter angle sweep was conducted.

Figure 7 shows the torque moment for the left root of the horizontal tail plane for each of the encounter angles. Interesting dynamics emerge, e.g. the maximum load levels for positive torque can occur at the first peak at $\psi \approx 90$ deg or at the second peak at around $\psi \approx 45$ deg. It becomes obvious that a comprehensive sweep study is required to determine the maximum loads. The primary objective of this study is to validate the unsteady

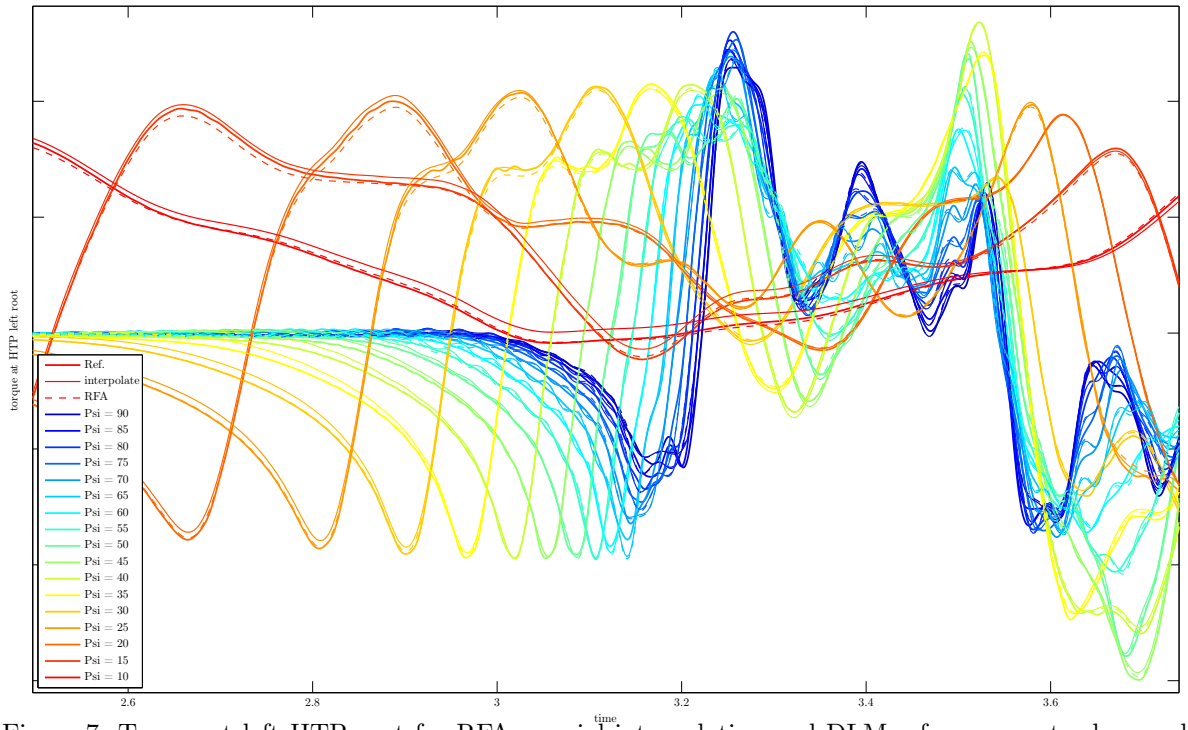

Figure 7: Torque at left HTP root for RFA, special interpolation and DLM reference unsteady aerodynamics

aerodynamics during wake vortex encounters. Two different methods for frequency interpolation of the AIC matrices $\mathbf{Q}_{gj}$ are compared. First, the common interpolation scheme base on a cubic radial base function as proposed in [23, 24]. This is the so called "special linear interpolation", where the imaginary part is divided by the reduced frequency before interpolation. Since this method has its roots in the PK-flutter method and is targeted

towards generalized aerodynamic forces, its suitability for response calculations should be under scrutiny.

Secondly, the RFA is evaluated at different reduced frequencies to determine whether the method is accurate enough. Basis for both interpolation schemes was a DLM calculation for 25 reduced frequencies, equally spaced for higher frequencies and bunched for frequencies from zero to 1.0. The RFA was conducted with 15 poles.

Additionally, reference DLM results were calculated at each of the 1024 frequency points used for the frequency domain calculation without any interpolation. The results are shown in figure 7.

Whilst not perfect, the RFA yields similar accuracy to the special interpolation. Both interpolation methods are capable of capturing the load levels accurately, when compared to the reference results. It can be concluded that the RFA is suited for response calculations even when high reduced frequencies are excited.

4.4 Position and Attitude Dependence of WVE

So far, the trajectories during the crossing of the wake, were pre-computed. Hence, no feedback regarding the position and attitude was considered. In [1] the case of $\Psi = 0$ deg revealed the importance of considering this dependency due to the large roll angles induced during the wake encounter.

With a similar sweep study as in the previous paragraph, the limits of these fixed path calculations are explored. The vertical offset h is chosen to be between the wing plane and the horizontal tail plane, to increase the rigid aircraft response in pitch. All subsequent calculations use the unsteady aerodynamics based on the RFA. First, the integral loads

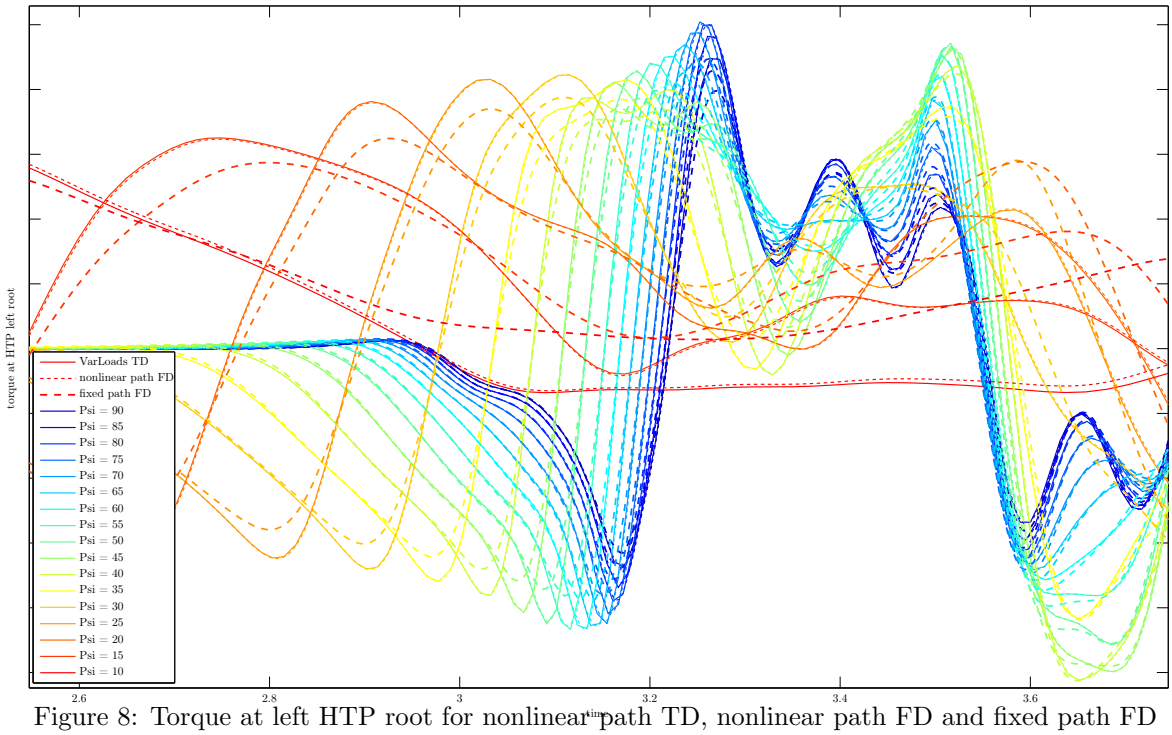

Figure 8: Torque at left HTP root for nonlinear path TD, nonlinear path FD and fixed path FD

model was simulated in the time domain. The resulting trajectory was used to generate an excitation spectrum as described in section 4.2. Finally, a frequency spectrum of a fixed path trajectory without feedback from the equations of motion is computed. Time responses for a load station are shown in figure 8.

The difference in loads for the time domain and the frequency domain simulations using the nonlinear trajectory are negligible, thus validating the ODE integration scheme and implementation of the integral loads model.

The responses for the fixed path calculation vary significantly. As expected, the differences are quite large for the acute encounter angles. Somewhat surprising is the considerable mismatch also for the obtuse encounter angles. This can be attributed to the strong gradients in the wind field, where even small perturbations of the trajectories can result in relatively large differences of induced velocities. Figure 9 shows the vortex tracks relative to the aircraft of the nonlinear response in black and the fixed path in red for $\Psi = 90$ deg. The markers depict the location of the double vortex system at $t \approx 3.25$ s, roughly when the maximum loads are reached. Table 1 summarizes the differences of the

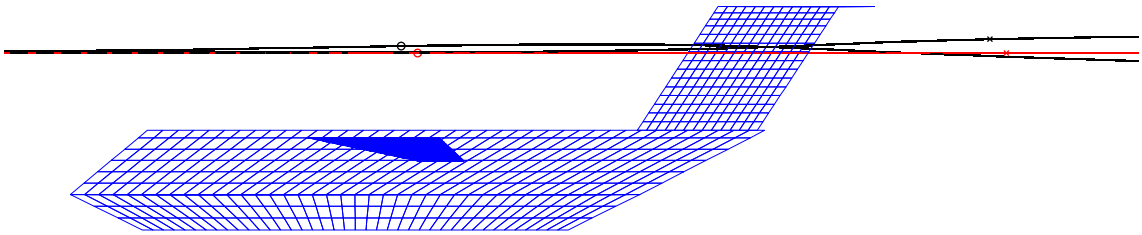

Figure 9: vortex trajectories for fixed and nonlinear path of a $\Psi = 90$ deg encounter

peak loads for the various encounter angles. For encounter angles around 45 deg, the

enc. angle Ψ [deg]	90	80	70	60	50	40	30	20	10
ratio peakloads [%]	12.7	11.7	10.2	6.7	-0.1	2.6	8.9	17.0	14.7

Table 1: ratio of peak loads for non-linear path to fixed path at different encounter angles

differences are smaller, because the maximum loads occur at the second peak, which is due to the dynamic response of the structure, rather than the impact of the vortex as for the first peak.

Depending on the scenario, the loads of wake vortex encounters can be significantly influenced by the nonlinear feedback of the equations of motion, even when only small perturbations are expected. When acute angles are considered, also large angles become important and require the consideration of nonlinear equations of motions.

5 CONCLUSIONS

The aim of this paper is to validate the integral load analysis model for wake vortex encounters proposed in [1], with an emphasis on theoretical and numerical considerations. In [25] a validation of such loads analysis models with recent flight test results is presented. The good agreement with flight test results corroborate the loads analysis based on the current modeling methodology.

Loads analysis models for wake vortex encounters require an unsteady aerodynamic model for considerably larger reduced frequencies compared to design gust calculations. Typically, the DLM is employed as unsteady aerodynamic method to generate frequency dependent AIC matrices. In [1] the DLM results were compared to incompressible unsteady pressure distributions, which were derived analytically in reference [19]. The present paper extends this comparison to the compressible regime. Since no analytical solutions for compressible pressure distributions exist, results of the DLM were compared to two different numerical solvers for compressible flow. Namely, a Possio solver and a velocity potential method for unsteady thin airfoils. The results show a good agreement up to moderate reduced frequencies for rigid body type excitations, i.e. heave, pitch and flap displacements. The 2D rigid body modes are associated with the structural dynamics and typically have a lower frequency range, when compared to the external excitation. Albeit, the required range is probably still larger than in the case of the design gust. The agreement for the sinusoidal gust input however was excellent even up to very high frequencies. As the requirement for high reduced frequencies originates mainly from the gust column, the DLM can be considered suitable for wake vortex encounters.

Further, a modification of the "physical" RFA (7) to address compressibility was presented. The added mass term disappears in favor of additional lag terms. The non-circulatory contribution can be determined explicitly by discretizing the airfoil with doublet panels, satisfying the Helmholtz equation (11). The limiting case for $Ma = 0$ yields the added mass term presented in [1]. The present RFA is also capable of accurately reproducing the spiralling behavior of the complex lift and moment for the flap excitations even for high reduced frequencies.

A frequency domain approach, determining the loads of a fixed path crossing of a wake vortex was established. The so called "special linear interpolation", which is classically used in response calculations and the "physical" RFA were compared to a reference DLM calculation without any interpolation for 1024 frequencies up to $k_{max} = 10$. Both interpolation schemes yielded a good agreement. The RFA had about the same accuracy as the special linear interpolation, when compared with the reference results.

Finally, the importance of the feed-back from the equations of motion, regarding the position and attitude relative to the vortex system was investigated. Nonlinear time domain simulations were compared to fixed path frequency domain calculations for a sweep of encounter angles. Remarkable is the fact, that not only for the acute angle, but even for the 90 degree encounters, a significant difference was found. This is due to large gradients in the velocity field, where also supposedly small differences can have a large impact on the resulting loads. It can be concluded that at least for some encounter scenarios, the online determination of the position relative to the vortices during the simulation is essential. This adds a nonlinear dependency, which is not tied to the nonlinearity of the equations of motion, but to the flow field with its large spatial gradients. The consideration of nonlinear equation of motion becomes necessary, when large roll angles are reached and the direction of the gravitational forces can no longer be neglected.

6 REFERENCES

[1] Kier, T.M. (2011). An Integrated Loads Analysis Model including Unsteady Aerodynamic Effects for Position and Attitude dependent Gust Fields. In *International*

Forum on Aeroelasticity and Structural Dynamics, IFASD-2011-052.

[2] European Aviation Safety Agency (2010). *Certification Specifications for Large Aeroplanes CS-25*, vol. Subpart C - Structure. EASA.

[3] J. Hofstee, T. Kier, C. Cerulli, G. Looye (2003). A Variable, Fully Flexible Dynamic Response Tool for Special Investigations (VarLoads). In *International Forum on Aeroelasticity and Structural Dynamics*.

[4] T. Kier, G. Looye and J. Hofstee (2005). Development of Aircraft Flight Loads Analysis Models with Uncertainties for Pre-Design Studies. In *International Forum on Aeroelasticity and Structural Dynamics*.

[5] Kier, T.M. and Looye, G.H.N. (2009). Unifying Manoeuvre and Gust Loads Analysis. In *International Forum on Aeroelasticity and Structural Dynamics*, IFASD-2009-106.

[6] R. J. Guyan (1965). Reduction of stiffness and mass matrices. *Journal of Aircraft*, 3(2), 380.

[7] M. R. Waszak and D. K. Schmidt (1986). On the flight dynamics of aeroelastic vehicles. In *AIAA Atmospheric Flight Mechanics Conference*, AIAA 86-2077. AIAA, pp. 120–133.

[8] M. R. Waszak and D. K. Schmidt (1988). Flight Dynamics of Aeroelastic Vehicles. *Journal of Aircraft*, 25(6), 563–571.

[9] M. R. Waszak, C. S. Buttrill and D. K. Schmidt (1992). Modeling and Model Simplification of Aeroelastic Vehicles: An Overview. Tech. Rep. NASA TM-107691, NASA LARC.

[10] C. Reschke (2006). *Integrated Flight Loads Modelling and Analysis for Flexible Transport Aircraft*. Ph.D. thesis, Universität Stuttgart.

[11] Hedman, S. (1965). Vortex Lattice Method for Calculation of Quasi Steady State Loadings on Thin Elastic Wings. Tech. Rep. Report 105, Aeronautical Research Institute of Sweden.

[12] Albano, E. and Rodden, W. (1969). A doublet-lattice method for calculating lift distributions on oscillating surfaces in subsonic flows. *AIAA Journal*, 7(2), 279–285.

[13] W.P. Rodden, J.P. Giesing and T.P. Kalman (1971). New developments and applications of the subsonic doublet-lattice method for nonplanar configurations. In *AGARD Symposium on unsteady aerodynamics for aeroelastic analyses of interfering surfaces*, AGARD-CP-80-71. AGARD.

[14] R.L. Harder and R.N. Desmarais (1972). Interpolation Using Surface Splines. *Journal of Aircraft*, 9(2), 189–191.

[15] Roger, K. L. (1977). Airplane math modeling methods for active control design. In *AGARD Structures and Materials Panel*, AGARD/CP-228. AGARD, pp. 4–1 – 4–11.

[16] Edwards, J.W. (1979). Applications of Laplace transform methods to airfoil motion and stability calculations. In *20th Structures, Structural Dynamics and Materials Conference*, AIAA 1979-772.

[17] I. Abel (1979). An analytical technique for predicting the characteristics of a flexible wing equipped with an active flutter-suppression system and comparison with wind-tunnel data. Tech. Rep. NASA TP-1367, NASA LARC.

[18] M. Karpel (1981). Design for Active and Passive Flutter Suppression and Gust Alleviation. Tech. Rep. NASA CR-3482, NASA.

[19] Knoblach, A. and Kier, T.M. (2011). Incompressible unsteady thin airfoil theory – revisited. Tech. Rep. DLR-IB 571-11/03, German Aerospace Centre, Institute of Robotics and Mechatronics.

[20] Carstens, V. (1975). Berechnung der instationären Druckverteilung an harmonisch schwingenden Gittern in ebener Unterschallströmung, Teil II. Tech. Rep. DFVLR IB 253-75J02.

[21] Hounsfield, C. (2012). Vortex surfing - ride the wave. *Aerospace Testing International*, November/December 2012, 50–53.

[22] Kauertz, S., Holzäpfel, F., and Kladetzke, J. (2012). Wake vortex encounter risk assessment for crosswind departures. *Journal of Aircraft*, 49, 281–291.

[23] W.P. Rodden, R.L. Harder, and E.D. Bellinger (1979). Aeroelastic Addition to NASTRAN. Tech. Rep. NASA CR-3094, NASA.

[24] W. P. Rodden and E. H. Johnson (1994). *MSC.Nastran Aeroelastic Analysis User's Guide*. MSC.

[25] Climent, H. et al. (2013). Flight test validation of wake vortex encounter loads. In *International Forum on Aeroelasticity and Structural Dynamics*, IFASD-2013-27B.